01 Dec 2005

A Novel Method for Determination of Dielectric Properties of Materials using a Combined Embedded Modulated Scattering and Near-Field Microwave Techniques-Part I: Forward Model

Dana M. Hughes

R. Zoughi
Missouri University of Science and Technology, zoughi@mst.edu

Recommended Citation

D. M. Hughes and R. Zoughi, "A Novel Method for Determination of Dielectric Properties of Materials using a Combined Embedded Modulated Scattering and Near-Field Microwave Techniques-Part I: Forward Model," *IEEE Transactions on Instrumentation and Measurement*, vol. 54, no. 6, pp. 2389-2397, Institute of Electrical and Electronics Engineers (IEEE), Dec 2005.
The definitive version is available at https://doi.org/10.1109/TIM.2005.858132

A Novel Method for Determination of Dielectric Properties of Materials Using a Combined Embedded Modulated Scattering and Near-Field Microwave Techniques—Part I: Forward Model

Dana Hughes and Reza Zoughi, *Senior Member, IEEE*

***Abstract*—The use of combined embedded modulated scattering technique and near-field microwave nondestructive testing techniques is investigated as a novel method for evaluating the dielectric properties of a material. The forward formulation for determining the reflection coefficient at the aperture of a waveguide radiating into a dielectric half-space in which a PIN diode-loaded dipole (i.e., modulated scattering technique probe) is embedded is presented. This formulation is based upon calculating the near-field coupling between the waveguide and the dipole as a mutual impedance.**

***Index Terms*—Dielectric material characterization, embedded sensors, microwave nondestructive testing, modulated scattering technique.**

I. Introduction

NEAR-field microwave nondestructive testing and evaluation (NDT&E) techniques have shown to be effective means for inspection of various materials and structures, with applications in the areas of civil infrastructure, industrial process control, materials evaluation, aeronautical, and naval applications [1]. Near-field microwave NDT techniques offer several advantages over traditional NDT techniques, and are often the ideal method to use when inspecting certain types of materials or structures (e.g., thick sandwich composite structures). Measurements may be performed in a one-sided and non-contact manner. Microwave signals are capable of penetrating into thick and layered dielectric slabs or half-spaces, and are sensitive to variations in the geometrical and material properties of the layers [2]. While microwave techniques are not capable of penetrating conducting materials, investigation of surface flaws in metals, such as the presence of corrosion, pitting or fatigue cracking is possible, either on bare metal, or under a layer of paint, primer, or a dielectric slab [3]–[5]. Near-field microwave measurements, using microwave probes, provide geometrical information about an interior flaw which correlates well with the spatial geometry of the structure under investigation, and interpretation of the microwave signal requires little or no operator expertise. Finally, microwave measurement devices may be designed to be robust, portable and low power, and capable of being used in harsh environments.

Extensive research into the investigation of cement-based structures has shown the capability of microwave techniques for determining several important parameters related to these structures, such as the water-to-cement (w/c), sand-to-cement (s/c), and course aggregate-to-cement (ca/c) ratios [6]–[9]. Furthermore, as these parameters are used to determine the compressive strength of cement-based materials, microwave measurements may be correlated to the compressive strength of a structure. As microwave techniques are sensitive to the chemical state of a material, these are ideal for cure-state monitoring of cement and other materials [7]. Microwave techniques are also very sensitive to the ingress of water and salt water, which may cause corrosion of steel reinforcement in cement-based structures [10]–[12].

Microwave techniques are also capable of investigating composite panels and sandwich structures. These techniques have been shown to be capable of determining the presence and spatial extent of delamination, disbond, and impact damage in these structures [2], [13], [14]. Furthermore, it is possible to accurately determine the thickness or dielectric properties of a composite panel, or a dielectric slab either backed by free-space or a metal plate [13]. As with cement-based materials, microwave techniques are also sensitive to the state of cure of the epoxy resin, as well as capable of detecting ingress of water in either foam or areas of impact damage [15]. Finally, the polarization of the microwave signal allows for determinations of the orientation of fibers in composites.

Microwave techniques, as described above, are based on determining the dielectric properties of a material, through the measurement of the reflected signal from a structure (i.e., the reflection coefficient). For near-field microwave NDT techniques, this is often measured at the aperture of an open-ended rectangular waveguide probe. The (relative to free-space) dielectric property of a material is a complex parameter (i.e., $\varepsilon_r = \varepsilon_r' - j\varepsilon_r''$) consisting of its permittivity (i.e., real part), which represents the material's ability to store microwave energy, and its loss factor (i.e., imaginary part), which represents the material's ability to absorb microwave energy. These parameters correlate to the chemical structure of the material under investigation, and, in the case of a material consisting of a mixture of

Manuscript received April 26, 2003; revised November 29, 2004. This work was supported in part by a Graduate Assistanceship in Areas of National Need Fellowship.

The authors are with the Electrical and Computer Engineering Departement, University of Missouri-Rolla, Rolla, MO 65409-0040 USA (e-mail: zoughi@ece.umr.edu).

Digital Object Identifier 10.1109/TIM.2005.858132

several constituents, may be represented as effective dielectric properties using an appropriate dielectric mixing model.

Currently, the dielectric properties of a material may be determined in a variety of ways using microwave NDT techniques [1]. The calculation of reflection coefficient of a rectangular waveguide radiating into a dielectric half-space, and the inverse problem of determining the dielectric constant of the half-space from its measured reflection coefficient, have been investigated, including consideration for the effects of higher order modes at the waveguide aperture [16]. The theoretical modeling of analyzing multilayered structures using both open-ended waveguides and coaxial probes has been investigated [17], [18]. Accurate determination of the dielectric properties of a section of waveguide filled with solid, liquid, or granular materials has also been formulated [19].

The combined use of near-field microwave NDT techniques, using an open-ended rectangular waveguide probe, and embedded modulated scattering technique (MST), using a PIN diode-loaded dipole, has been proposed as a novel means of determining the dielectric properties of a material in which the probe is embedded [20]. Previous investigations have produced encouraging results, showing that this technique would be a potentially beneficial addition to the toolbox of dielectric property characterization of materials [21]. This technique would allow for embedding a probe in critical locations within a structure for more sensitive measurements at the areas of interest. Furthermore, as this probe remains embedded in the structure, the presence of defects or variations in the material may be monitored over time, in order to observe changes in the properties of a defect or dielectric property change in the material.

The proposed embedded MST technique has several advantageous attributes over other techniques [21], [22]. The technique allows for localized measurement of the dielectric properties of a material. Thus, the probe may be placed in a critical location, such as near a rebar or a composite joint, where sensitive measurements are necessary. Furthermore, the signal from the MST probe can be easily distinguished (as will be seen) and since the measurements are coherent (i.e., magnitude and phase), averaging over a short period of time increases the signal-to-noise ratio of the measurements significantly. This allows for an increase in the sensitivity of the measurement. Finally, the use of an array of probes allows for rapid measurement over a large area.

II. Approach

For this investigation, a thin, near-resonant dipole, centrally loaded with a PIN diode (i.e., the MST probe), is embedded in an infinite half-space of a material, as shown Fig. 1. The PIN diode is modulated between a forward- and reverse-biased state using a pair of thin modulation wires connected to a square-wave generator operating at a low frequency (i.e., 0.5 to a few hertz). The load impedance modulates between a forward- and reverse-biased impedance as a function of time. Thus, a microwave signal incident upon the MST probe will be scattered while tagged with this modulation waveform.

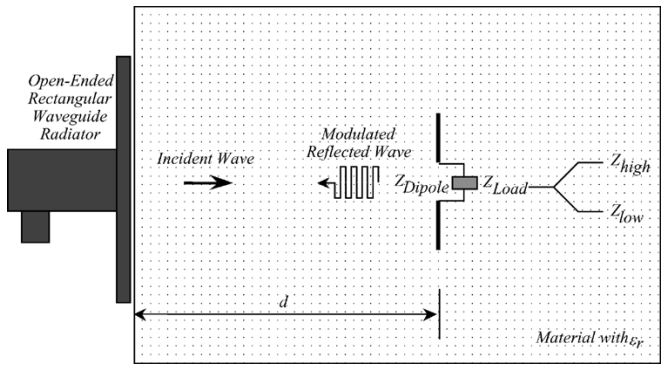

Fig. 1. Geometry of an MST probe embedded in a dielectric half-space and illuminated by an open-ended rectangular waveguide radiator.

As seen in Fig. 1, the MST probe is illuminated by an open-ended rectangular waveguide, which is located at the surface of the half-space and calibrated at the plane of the aperture. The incident field from the waveguide radiator will be scattered by the MST probe, part of which will propagate back, encoded or tagged with the modulation waveform, to the aperture of the waveguide. This provides for a modulated reflection at the aperture, which combines with the static reflection due to the boundary between the surface of the dielectric half-space and the waveguide aperture. Fig. 2 shows an example of the magnitude and phase of the modulated reflection coefficient, over several cycles of the modulation waveform, with the MST probe embedded in a half-space of fine sand. Fig. 2 shows the reflection coefficient measured by an HP8510C vector network analyzer (VNA) for a time span of about 10 seconds. During this time the VNA recorded 401 measurement points [as labeled in the horizontal axes of Fig. 2(a) and (b)]. Approximately half of these points correspond to the high state reflection coefficient and the other half to the low state (as shown).

III. Formulation of the Forward Problem

The forward formulation of calculating the modulated reflection coefficient measured at the aperture of the waveguide, in the presence of an embedded MST probe, is based on calculating the coupling between the waveguide aperture and the embedded dipole everywhere, including the near-field of the waveguide radiator [21]. The formulation presented here is general in terms of the near- and far-field regions of the waveguide radiator and is valid for all locations of the MST probe relative to the waveguide radiator. In this investigation, this is performed by calculating the mutual impedance between the two using the induced electromotive force method [21], [23], [24]. This requires the knowledge of the radiated fields from the first antenna (i.e., the waveguide aperture) and the ideal current distributions on the second antenna (i.e., the dipole) due to a signal fed at the terminal of the first antenna (i.e., the waveguide radiator). This technique assumes the material is linear and isotropic (i.e., the relationship between the waveguide radiator and MST probe is reciprocal), and requires a well-defined port for both antennas, which is the case both with a waveguide aperture and a dipole antenna.

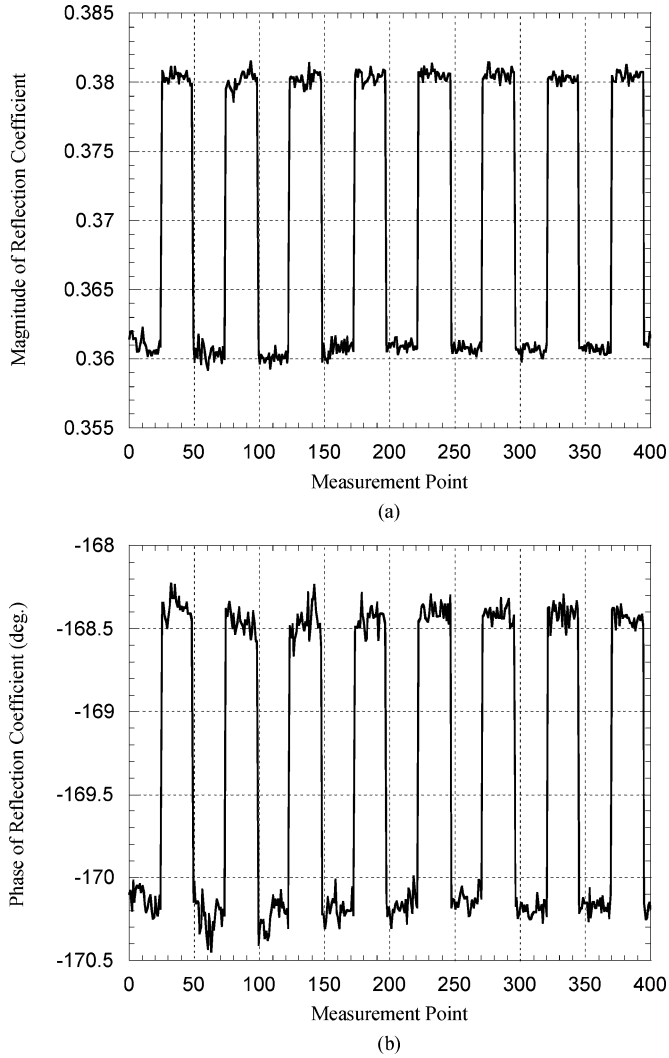

Fig. 2. Example of the (a) magnitude and (b) phase of the modulated reflection coefficient over several cycles of the modulation waveform.

A. Radiation From a Waveguide Aperture

The far-field radiation from an open-ended rectangular waveguide aperture has been determined in the past based on calculating the equivalent currents on the aperture, and the radiated electric and magnetic fields from the vector potentials due to these currents [25]. Here, a similar approach is used; however, the near-field components of the radiated fields are included in the derivation in order for these to be valid at all locations in front of the waveguide radiator. The center of the waveguide aperture is located at the origin, with the broad dimension (i.e., a) of the waveguide orientated along the x axis and the narrow dimension (i.e., b) along the y axis, as in Fig. 3.

For most applications, the flange may be considered an infinite ground plane. While any waveguide mode may be used in this investigation, dominant (i.e, TE_{10}) mode is used here. The tangential electric and magnetic field distributions on the aperture are given as

$$\overline{E}_y^{ap}(x',y') = (1+\Gamma_s)V_{11}\overline{e}_y(x',y') \tag{1a}$$
$$\overline{H}_x^{ap}(x',y') = (1-\Gamma_s)V_{11}\overline{h}_x(x',y') \tag{1b}$$

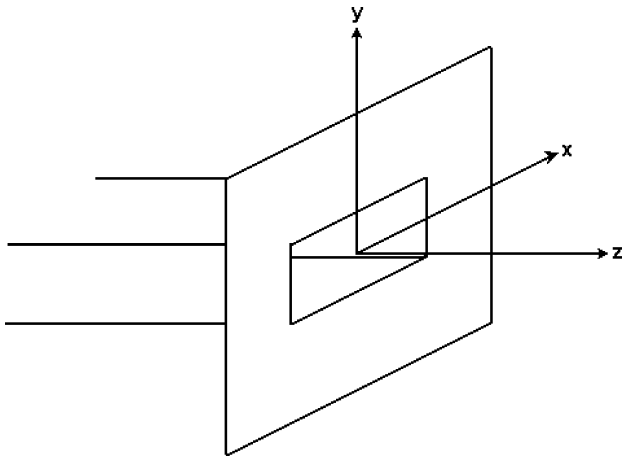

Fig. 3. Geometry and coordinate system for a waveguide aperture mounted on a flange.

where V_{11} is defined as the complex amplitude coefficient representing the magnitude and phase of the electric and magnetic field at the aperture of the waveguide, which may be considered the voltage at the aperture. The characteristic impedance of the waveguide is present in the orthonormal distribution of the tangential magnetic fields. Γ_s is the reflection coefficient at the aperture of the waveguide radiating into a half-space of the material (i.e., without the MST probe), and may be measured or calculated using a variety of method previously investigated, and will not be described here [16], [17]. e_y and h_x are the tangential orthonormal electric and magnetic field distributions for the dominant mode and are given as [26], [27]

$$\overline{e}_y(x',y') = -\sqrt{\frac{2}{ab}}\sin\left(\frac{\pi}{a}x' + \frac{\pi}{2}\right) \tag{2a}$$
$$\overline{h}_x(x',y') = \frac{1}{Z_0}\sqrt{\frac{2}{ab}}\sin\left(\frac{\pi}{a}x' + \frac{\pi}{2}\right) \tag{2b}$$

the characteristic impedance of the waveguide Z_0 is given as

$$Z_0 = \frac{k\eta}{\beta} \tag{3}$$

where η is the intrinsic impedance of the material filling the waveguide, and

$$\beta = \sqrt{k^2 - k_c^2} \tag{4}$$

and

$$k_c = \frac{\pi}{a}. \tag{5}$$

From the electric and magnetic field distributions given in (1a) and (1b), the equivalent electric and magnetic currents on the aperture of the waveguide are given as

$$\overline{J}_s = \hat{n} \times \overline{H}^{ap} = \hat{z} \times \overline{H}^{ap} \tag{6a}$$
$$\overline{M}_s = -\hat{n} \times \overline{E}^{ap} = -\hat{z} \times \overline{E}^{ap}. \tag{6b}$$

As the flange of the waveguide is considered an infinite ground plane, the introduction of the image of these currents simplifies

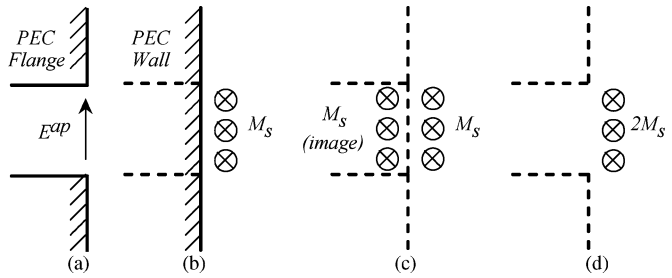

Fig. 4. (a) Electric current distribution on the aperture of the waveguide, (b) equivalent magnetic current distribution for this, (c) removal of the infinite ground plane and inclusion of the image current, and (d) combination of the equivalent current and an image current.

the derivations. This results in a doubling of the magnetic current, and nullification of the electric current, as shown in Fig. 4 [28].

The electric vector potential may be determined at a point outside the aperture by

$$\overline{F}(x,y,z) = \frac{\varepsilon}{4\pi}\int\int_S \overline{M}_s(x',y')\frac{e^{-jkR}}{R}ds' \tag{7}$$

where k and R are given by

$$k = \omega\sqrt{\mu_0\varepsilon_0(\varepsilon_r' - j\varepsilon_r'')} \tag{8}$$

and

$$R = \sqrt{(x-x')^2 + (y-y')^2 + z^2}. \tag{9}$$

The primed coordinates are the source coordinates on the aperture of the waveguide, and the unprimed coordinates are the observation coordinates outside of the aperture.

From these, the electric and magnetic fields outside the aperture can be calculated by

$$\overline{E}_F(x,y,z) = -\frac{1}{\varepsilon}\nabla\times\overline{F}(x,y,z) \tag{10a}$$

$$\overline{H}_F(x,y,z) = -j\frac{1}{\omega\mu\varepsilon}\left[k^2\overline{F}(x,y,z) + \nabla(\nabla\cdot\overline{F}(x,y,z)\right]. \tag{10b}$$

Substituting (1), (6b), and (7) into the above, and accounting for the image of the magnetic current (i.e., doubling this value), the total fields radiated by a flange-mounted aperture are as shown in (11a)–(11e) at the bottom of the page. Finally, if the mode voltage V_{11} is expressed explicitly in the equations, the electric and magnetic field distributions for the orthonormal modes on the aperture e^i and h^i can be defined and are given by

$$\overline{E}(x,y,z) = V_{11}\overline{e}^i(x,y,z) \tag{12a}$$

$$\overline{H}(x,y,z) = V_{11}\overline{h}^i(x,y,z). \tag{12b}$$

Details of this derivation, including the derivation for higher order modes, are available elsewhere and will not be repeated here [21].

B. Determination of the Current Distribution on the Dipole

In order to calculate the ideal current distribution on a dipole embedded in a generally lossy media, the method of moments may be employed in conjunction with the Pocklington's integral equation for the scattering from a thin wire antenna [29]–[31]. For this, a thin dipole antenna, orientated along the z axis and centered at the origin, with a voltage drop across a delta-gap at the center of the dipole, is located in a generally lossy material, as shown in Fig. 5. The dipole has length l and radius a, and the

$$E_y(x,y,z) = -\frac{1}{2\pi}\int_{x'=-a/2}^{a/2}\int_{y'=-b/2}^{b/2} E_y^{ap}(x',y')\times\frac{e^{-jkR}}{R^3}(-jkR-1)(z)dy'dx' \tag{11a}$$

$$E_z(x,y,z) = \frac{1}{2\pi}\int_{x'=-a/2}^{a/2}\int_{y'=-b/2}^{b/2} E_y^{ap}(x',y')(y-y')\times\frac{e^{-jkR}}{R^3}(-jkR-1)dy'dx' \tag{11b}$$

$$H_x(x,y,z) = \frac{j}{2\pi\omega\mu}\cdot\int_{x'=-a/2}^{a/2}\int_{y'=-b/2}^{b/2}\left\{-k^2E_y^{ap}(x',y')\frac{e^{-jkR}}{R} - E_y^{ap}(x',y')(x-x')^2\frac{e^{-jkR}}{R^5}(-k^2R^2+j3kR+3) + E_y^{ap}(x',y')\frac{e^{-jkR}}{R^3}(jkR+1)\right\}dy'dx' \tag{11c}$$

$$H_y(x,y,z) = \frac{-j}{2\pi\omega\mu}\int_{x'=-a/2}^{a/2}\int_{y'=-b/2}^{b/2} E_y^{ap}(x',y')(x-x')(y-y')\times\frac{e^{-jkR}}{R^5}(-k^2R^2+j3kR+3)dy'dx' \tag{11d}$$

$$H_z(x,y,z) = \frac{-j}{2\pi\omega\mu}\int_{x'=-a/2}^{a/2}\int_{y'=-b/2}^{b/2} E_y^{ap}(x',y')(x-x')z\times\frac{e^{-jkR}}{R^5}(-k^2R^2+j3kR+3)dy'dx' \tag{11e}$$

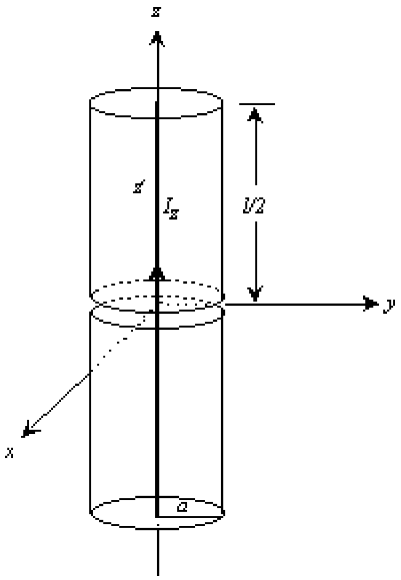

Fig. 5. Current distribution on a dipole of length l and radius a due to a voltage fed at the center terminal.

voltage fed at the terminal port (i.e., at the center of the dipole) is V_{22}.

The current distribution along the length of a dipole, due to an incident electric field, can be expressed as an integral equation as [25]

$$\int_{-1/2}^{1/2} I_z(z')\frac{e^{-jkR}}{4\pi R^5}\left[(1+jkR)(2R^2-3a^2)+(kaR)^2\right]dz' = -j\omega\varepsilon_0(\varepsilon_r'-j\varepsilon_r'')E_z^i(\rho=a,z) \quad (13)$$

where $I_z(z')$ is the current distribution along the center of the dipole and R is the distance from a source point on the line of current to an observation point on the surface of the wire, and is given as

$$R=\sqrt{a^2+(z-z')^2} \quad (14)$$

for a sufficiently thin wire and $E^i(\rho=a,z)$ is generally the incident electric field on the surface of the wire. In this investigation, this will consist of only the electric field at the center of the wire due to the voltage drop at the feed terminal.

The current distribution in the integral equation can be determined though the application of the method of moments [29]. The dipole is divided into N segments, and the current on each segment is approximated using a set of basis functions, and the associated coefficients for the basis functions are determined by satisfying the electric field in (13) at each segment. For this investigation, the current is approximated using a set of piecewise functions, namely

$$I_z(z')\cong\sum_{n=0}^{N-1} I_n g_n(z') \quad (15)$$

where $g_n(z')$ is the basis function for the dipole, given by

$$g_n(z')=\begin{cases}1, & z_n-\frac{\Delta z}{2}\le z'\le z_n+\frac{\Delta z}{2}\\ 0, & otherwise\end{cases} \quad (16)$$

and Δz is the segment length given by

$$\Delta z=\frac{l}{N}. \quad (17)$$

The electric field across the delta-gap due to the voltage drop across it is tested using collocation (i.e., a Dirac delta function at the center of the segment).

Applying the set of basis and testing functions to (13), the problem may be expressed as a set of N linear equations with N solutions, and may be expressed as

$$\left[\overline{Z}\right]\left[\overline{I}\right]=\left[\overline{V}\right] \quad (18)$$

where I is an N element vector consisting of the approximations for the current at each segment, Z is an $N\times N$ matrix representing the impedance between two segments along the dipole, given as shown in (19) at the bottom of the page.

Finally, V is an N element vector representing the testing function for the voltage fed at the terminal and is given as

$$V_m=\begin{cases}-j\omega\varepsilon_0(\varepsilon_r'-j\varepsilon_r'')\frac{1}{\Delta z}, & m=p\\ 0, & otherwise\end{cases}. \quad (20)$$

In order to determine the current distribution, the impedance matrix in (18) is inverted and multiplied by the solution, namely

$$\left[\overline{I}\right]=\left[\overline{Z}\right]^{-1}\left[\overline{V}\right]. \quad (21)$$

This provides for the coefficients for the current approximation I_n, given in (15), from which the current distribution may be determined. If the voltage is expressed explicitly, an admittance function along the length of the dipole may relate this current to the voltage fed at the delta-gap, given as [21]

$$I_z(z)=V_{22}Y_z(z). \quad (22)$$

$$Z_{mn}=\int_{z_n-\Delta z/2}^{z_n+\Delta z/2}\frac{e^{-jkR(z_m,z')}}{4\pi R(z_m,z')^5}\times\left[(1+jkR(z_m,z'))(2R(z_m,z')^2-3a^2)+(kaR(z_m,z'))^2\right]dz' \quad (19)$$

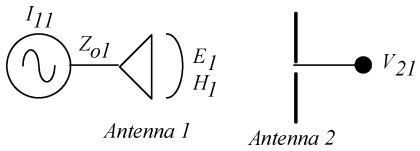

Fig. 6. Geometry of the combined circuit and electromagnetic form of the reciprocity theorem applied to two antennas.

C. Calculation of the Mutual Impedance Between the Waveguide Aperture and Dipole

Several methods for calculating the mutual impedance between two antennas have been investigated in the past [23], [24], [32]–[35]. Here, a mixed form of the reciprocity theorem is employed. The reciprocity theorem in pure circuit form relates two ports of a circuit as

$$V_{12}I_{11} = V_{21}I_{22}. \tag{23}$$

In pure electromagnetic form, the reciprocity theorem represents the interaction between two antennas, as shown in Fig. 6. This may be expressed in its most general and useful form as

$$\iiint_V \left(\overline{E}_1 \cdot \overline{J}_2 - \overline{H}_1 \cdot \overline{M}_2\right) dv = \iiint_V \left(\overline{E}_2 \cdot \overline{J}_1 - \overline{H}_2 \cdot \overline{M}_1\right) dv \tag{24}$$

which gives rise to the idea of the reaction between two antennas, expressed as $\langle 1,2 \rangle$, and is defined as

$$\langle 1,2 \rangle = \iiint_V \left(\overline{E}_1 \cdot \overline{J}_2 - \overline{H}_1 \cdot \overline{M}_2\right) dv \tag{25a}$$

$$\langle 2,1 \rangle = \iiint_V \left(\overline{E}_2 \cdot \overline{J}_1 - \overline{H}_2 \cdot \overline{M}_1\right) dv. \tag{25b}$$

The combined form of the reciprocity theorem relates the radiated fields from one antenna to the voltage and current on the port of another [23], represented by

$$V_{21}I_{22} = -\langle 1,2 \rangle. \tag{26}$$

This allows for the expression of the mutual impedance between the two antennas given by

$$Z_{21} = \frac{V_{21}}{I_{11}} = \frac{-1}{I_{11}I_{22}} \iiint_V \left(\overline{E}_1 \cdot \overline{J}_2 - \overline{H}_1 \cdot \overline{M}_2\right) dv. \tag{27}$$

Considering the dipole as antenna 2, the electric current density J_2 consists only of the line current given in (22). This simplifies (27) to

$$Z_{21} = \frac{-1}{I_{11}I_{22}} \int_{-1/2}^{1/2} \overline{E}_1 \cdot \overline{I}_2 dz. \tag{28}$$

Explicitly expressing the voltage incident in the waveguide and across the feed gap of the dipole, as in (12) and (22), the voltages may be taken outside the integral, and combined with the current variables, resulting in

$$Z_{21} = -Z_{11}Z_{22} \int_{-1/2}^{1/2} e_1^{-i}(z) \cdot \overline{Y}_2(z) dz. \tag{29}$$

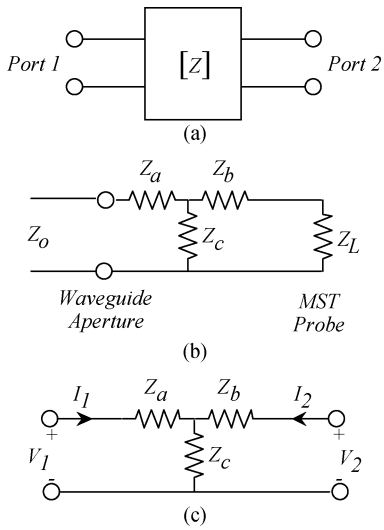

Fig. 7. (a) Representation of the interaction of the two antennas as an impedance network, (b) equivalent T-network for this, and (c) equivalent loaded transmission line, when considering the load impedance and waveguide feed.

This provides for the mutual impedance between the waveguide aperture and dipole antenna in well-defined terms.

D. Impedance Matrix Representation and Reflection Coefficient Calculation

The interaction between the waveguide port (i.e., the aperture) and the terminal port of the dipole may now be expressed in terms of an impedance matrix, as shown in Fig. 7(a). Since the material in which the dipole is embedded is assumed to be linear and isotropic (i.e., the relationship between the waveguide aperture and dipole is reciprocal), the mutual impedance between these two ports is the same (i.e., $Z_{21} = Z_{12}$). This allows for the impedance matrix to be expressed as a T-network, as shown in Fig. 7(b) [27]. Attaching the load impedance Z_L, (i.e., the PIN diode) at port 2 and the waveguide feed at port 1, with characteristic impedance Z_o, the interaction between the two antennas becomes a loaded transmission line problem, as in Fig. 7(c).

The values for the impedance matrix of the T-network in Fig. 7(b) can be calculated as

$$Z_{11} = Z_a + Z_c \tag{30a}$$

$$Z_{12} = Z_{21} = Z_c \tag{30b}$$

$$Z_{22} = Z_b + Z_c \tag{30c}$$

where Z_{11} and Z_{22} are the input impedances of the waveguide aperture and dipole, respectively, and Z_{21} is the mutual impedance between the two, as given in (29). The input impedance for the dipole can be calculated from the method of moments formulation given earlier, and the input impedance of the waveguide aperture can be calculated from the measured static reflection coefficient, which is the reflection coefficient at the aperture of the waveguide without the MST probe present (i.e., the waveguide is radiating in a half-space of the dielectric material). This reflection coefficient may either be measured or calculated using a previously established method [16], [17].

Z_a, Z_b, and Z_c can be calculated from (30a)–(30c) and are the impedance values used in the T-network. With the load impedance attached, as in Fig. 7(c), the total input impedance of the waveguide aperture (i.e., the input impedance with the MST probe present) can be calculated as

$$Z_{in} = Z_a + \frac{Z_c(Z_b + Z_L)}{Z_b + Z_c + Z_L} \tag{31}$$

from which the reflection coefficient can be calculated as

$$\Gamma = \frac{Z_{in} - Z_0}{Z_{in} + Z_0} \tag{32}$$

which can be used to calculate the modulated reflection coefficient for the forward- and reverse-biased states of the MST probe.

IV. Measurement Results for the Forward Formulation

To demonstrate the potential of this proposed technique, measured and calculated results were compared for the case of an MST probe in free-space and when embedded in fine sand, respectively. For this, the MST probe was centrally loaded with a commercially available PIN diode [36].

A. Free-Space Measurements

Free-space measurements were made at 10 GHz using an X-band waveguide radiator, with an MST probe located at several distances in front of the waveguide. The probe consisted of a 1.5-cm-thin dipole antenna loaded with a PIN diode. At this frequency, the forward- and reverse-biased impedance of the PIN diode are approximately $10+j70\ \Omega$ and $20-j20\ \Omega$, respectively [36], [37]. For this case, the static reflection coefficient was measured to be $\Gamma_s = 0.233\angle -75.4^\circ$ using an HP8510C vector network analyzer with the waveguide radiator calibrated at its aperture. Static reflection coefficient refers to the reflection coefficient measured at the rectangular waveguide aperture in the absence of an MST probe (i.e., rectangular waveguide aperture radiating into free-space). Calibration refers to the measurements having been referenced to the rectangular waveguide aperture as opposes to the input of the network analyzer. This is a standard procedure and is accomplished by using well-characterized waveguide loads (short, matched, and line extension).

Fig. 8(a) and (b) shows the magnitude and phase of reflection coefficient, measured at the aperture of the waveguide, as a function of the distance between the waveguide and the MST probe, along the center of the aperture (see Fig. 1). As can be seen, the measured values compare well with the calculated values, except when the MST probe is very near the radiating waveguide aperture.

The discrepancy between the measured and calculated values near the waveguide may be primarily attributed to the theoretical formulation not accounting for multiple reflections between the MST probe and the waveguide flange. This may be accounted for by modeling the image of the dipole due to the ground plane (i.e., the flange of the waveguide). Also, accounting for higher order modes may provide for some variation when near the aperture of the waveguide. Further discrepancy may be due to numerical errors in integration, as well as approximation of the current distribution on the dipole.

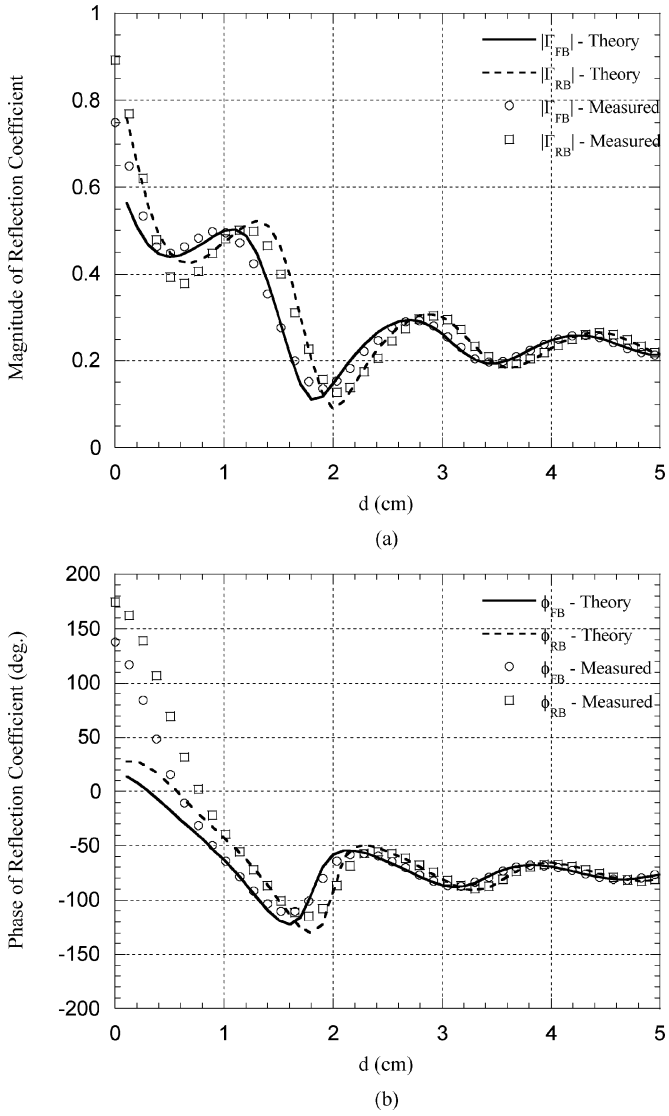

Fig. 8. Comparison of the measured and calculated (a) magnitude and (b) phase of forward- (FB) and reverse-biased (RB) reflection coefficient.

B. Dielectric Half-Space Measurements

Comparisons between the measured and calculated reflection coefficient values for an MST probe embedded in a half-space of fine sand, at S-band (2.6–3.95 GHz), were also conducted. The average dielectric constant of sand over S-band was measured using a two-port completely filled waveguide technique to be $\varepsilon_r = 2.76 - j0.03$ [19]. Measurements were made using a large enough volume of sand so that it could be considered a half-space, with an MST probe of length $l = 2.3$ cm embedded at a depth (i.e., d) of 5 cm.

Table I shows the measured static reflection coefficient, and the forward- and reverse-biased impedance values for the PIN diode used, and shows this comparison between the measured

TABLE I
COMPARISONS OF CALCULATIONS AND MEASUREMENTS AT 3 GHZ FOR SAND

ε_r'-$j\varepsilon_r$"	2.76-j0.03	Z_{fwd}	4.47 + j53.2 Ω
Γ_s (meas)	0.385∠-166.25°	Z_{rev}	1.71 - j70.7 Ω
Γ_{fwd} (meas)	0.364∠-169.09°	Γ_{fwd} (calc)	0.377∠-169.23°
Γ_{rev} (meas)	0.384∠-167.89°	Γ_{rev} (calc)	0.385∠-167.24°

TABLE II
COMPARISONS OF CALCULATIONS AND MEASUREMENTS AT 3.5 GHZ FOR SAND

ε_r'-$j\varepsilon_r$"	2.76-j0.03	Z_{fwd}	4.93 + j65.2 Ω
Γ_s (meas)	0.337∠-165.92°	Z_{rev}	1.83 - j50.3 Ω
Γ_{fwd} (meas)	0.356∠-161.79°	Γ_{fwd} (calc)	0.362∠-160.68°
Γ_{rev} (meas)	0.312∠-164.76°	Γ_{rev} (calc)	0.317∠-164.20°

and calculated forward- and reverse-biased reflection coefficients at 3 GHz [36], [37]. As can be seen, the measured and calculated values agree well.

Measurements were conducted at 3.5 GHz as well. Table II summarizes the parameters used in the measurements, and shows the comparison between the measured and calculated forward- and reverse-biased reflection coefficients at 3.5 GHz. Again, the measured and calculated values agree well.

From the results shown for both free-space and when the MST probe is embedded in a half-space of sand, the forward model provides for an accurate means of calculating the modulated reflection coefficient. Some discrepancy between the measured and calculated values in free-space exists when the MST probe is very near the waveguide aperture. This is primarily due to a) not considering the image of the dipole due to the flange of the waveguide and b) not taking higher order modes into account. As observed, this effect reduces rapidly as the distance between the waveguide and probe increases (i.e., d). Thus, this effect may not be an issue for the case of an embedded probe in practice, as the probe is usually embedded a few centimeters inside the material. Additional potential error in the calculated reflection coefficient may arise from inaccurate measurement of the static reflection coefficient at the radiating waveguide aperture. It has been observed that the modulated reflection coefficient is sensitive to variations in this value [38]. This poses a potential problem for materials that are inhomogeneous or contain scattering objects, as these will cause variations in the static reflection coefficient as a function of the position of the waveguide radiator. However, this problem may be overcome by averaging the measurement over several locations on the dielectric half-space.

V. CONCLUSION

The formulation of the reflection coefficient at the aperture of an open-ended rectangular waveguide, radiating into a dielectric half-space in which an MST probe, consisting of a dipole centrally loaded with a PIN diode, is embedded was presented. This formulation provides for a novel means of measuring the dielectric properties of a material at microwave frequencies and provides for an additional tool for material evaluation (as described in detail in Part II of this paper). This formulation is based upon the interaction between the waveguide and dipole probe, which is calculated utilizing the reciprocity theorem in electromagnetics. The formulation of the forward model is based upon this theorem, which was presented here.

The measurements conducted using an MST probe in free-space and in sand agree very well with the calculations from the model. This shows the validity of the forward model, and the potential for using this technique in the investigation of dielectric materials.

As mentioned earlier, there are several advantages to using this technique over traditional microwave measurements. The MST probe may be placed in critical locations inside a structure, which would focus the measurement around these areas. The modulated signal may be coherently measured and averaged, which increases the signal-to-noise ratio and ultimately the sensitivity of the measurements. Finally, arrays of MST probes may be used to investigate large regions.

As shown with the free-space measurements, there is a discrepancy between the measured and calculated values when the MST probe is very near the waveguide. This is primarily attributed to not accounting for the multiple reflections between the waveguide and MST probe and the higher order modes. This may be accounted for by including the image of the dipole due to the waveguide flange, which would affect the current distribution and input impedance of the dipole itself and the higher order modes. Also, it was observed that the measurements were sensitive to variations in the static reflection coefficient. Thus, this measurement needs to be an accurate representation of the material in front of the probe. This may require an average measurement of this reflection coefficient.

REFERENCES

[1] R. Zoughi, *Microwave Non-Destructive Testing and Evaluation*. Dordrecht, The Netherlands: Kluwer Academic, 2000.

[2] S. Bakhtiair, S. Ganchev, N. Qaddoumi, and R. Zoughi, "Microwave noncontact examination of disbond and thickness variation in stratified composite media," *IEEE Trans. Microwave Theory Tech.*, vol. 42, pp. 389–395, Mar. 1994.

[3] C. Huber, H. Abiri, S. Ganchev, and R. Zoughi, "Modeling of surface hairline crack detection in metals under coatings using open-ended rectangular waveguides," *IEEE Trans. Microwave Theory Tech.*, vol. 45, pp. 2049–2057, Nov. 1997.

[4] D. Hughes, R. Zoughi, R. Austin, N. Wood, and R. Engelbart, "Near-field microwave detection of corrosion precursor pitting under thin dielectric coatings in metallic substrate," in *Proc. 29th Annu. Review Progress Quantitative Nondestructive Evaluation*, vol. 22A, Bellingham, WA, Jul. 14–19, 2002, pp. 443–448.

[5] N. Qaddoumi, L. Handjojo, T. Bigelow, J. Easter, A. Bray, and R. Zoughi, "Microwave corrosion detection using open-ended rectangular waveguide sensors," *Mater. Eval.*, vol. 58, no. 2, pp. 178–184, Feb. 2000.

[6] K. Bois, A. Benally, and R. Zoughi, "Microwave near-field reflection property analysis of concrete for material content determination," *IEEE Trans. Instrum. Meas.*, vol. 49, pp. 49–55, Feb. 2000.

[7] K. J. Bois, A. D. Benally, P. S. Nowak, and R. Zoughi, "Cure-state monitoring and water-to-cement ratio determination of fresh Portland cement based materials using near-field microwave techniques," *IEEE Trans. Instrum. Meas.*, vol. 47, pp. 628–637, Jun. 1998.

[8] K. Bois, A. Benally, P. S. Nowak, and R. Zoughi, "Microwave nondestructive determination of sand to cement (s/c) ratio in mortar," *Res. Nondestructive Eval.*, vol. 9, no. 4, pp. 227–238, Apr. 1997.

[9] K. Mubarak, K. J. Bois, and R. Zoughi, "A simple, robust and on-site microwave technique for determining water-to-cement (w/c) ratio of fresh Portland cement-based materials," *IEEE Trans. Instrum. Meas.*, vol. 50, pp. 1255–1263, Oct. 2001.

[10] K. Bois, A. Benally, and R. Zoughi, "Near-field microwave noninvasive determination of NaCl in mortar," *Proc. Inst. Elect. Eng. Sci., Meas. Technol. (Special Issue on Non-Destructive Testing and Evaluation)*, vol. 148, no. 4, pp. 178–182, Jul. 2001.

[11] S. Peer, J. T. Case, E. Gallaher, K. E. Kurtis, and R. Zoughi, "Microwave reflection and dielectric properties of mortar subjected to compression force and cyclically exposed to water and sodium chloride solution," *IEEE Trans. Instrum. Meas.*, vol. 52, pp. 111–118, Feb. 2003.
[12] J. Case, S. Peer, K. Donnell, D. Hughes, R. Zoughi, and K. E. Kurtis, "Investigation of microwave reflection properties of mortar exposed to wet-dry cucles of tap water and chloride bath," in *Proc. 28th Annu. Review Progress Quantitative Nondestructive Evaluation*, vol. 21B, Brunswick, ME, Jul.-Aug. 29–3, 2001, pp. 1269–1276.
[13] S. Gray and R. Zoughi, "Dielectric sheet thickness variation and disbond detection in multi-layered composites using an extremely sensitive microwave approach," *Mater. Eval.*, vol. 55, no. 1, pp. 42–48, 1997.
[14] E. C. Greenawald, L. J. Levenberry, N. Qaddoumi, A. McHardy, R. Zoughi, and C. F. Poranski, "Microwave NDE of impact damaged fiberglass and elastomer layered composites," in *Proc. 26th Annu. Review Progress Quantitative Nondestructive Evaluation*, vol. 19B, Montreal, PQ, Canada, Jul. 25–30, 1999, pp. 1263–1268.
[15] N. Qaddoumi, S. Ganchev, and R. Zoughi, "Microwave diagnosis of low density glass fibers with resin binder," *Rese. Nondestruct. Eval.*, vol. 8, no. 3, pp. 177–188, 1996.
[16] K. J. Bois, A. D. Benally, and R. Zoughi, "Multimode solution for the reflection properties of an open-ended rectangular waveguide radiating into a dielectric half-space: The forward and inverse problems," *IEEE Trans. Instrum. Meas.*, vol. 48, pp. 1131–1140, Dec. 1999.
[17] S. Bakhtiari, S. Ganchev, and R. Zoughi, "A generalized formulation for admittance of an open-ended rectangular waveguide radiating into stratified deielectrics," *Res. Nondestruct. Eval.*, vol. 7, no. 2/3, pp. 75–87, 1995.
[18] ——, "Analysis of the radiation of an open-ended coaxial line into stratified dielectrics," *IEEE Trans. Microwave Theory Tech.*, vol. 42, pp. 1261–1267, Jul. 1994.
[19] K. Bois, L. Handjojo, A. Benally, K. Mubarak, and R. Zoughi, "Dielectric plug-loaded two-port transmission line measurement technique for dielectric property characterization of granular and liquid materials," *IEEE Trans. Instrum. Meas.*, vol. 48, pp. 1141–1148, Dec. 1999.
[20] A. Joisel, K. J. Bois, A. D. Benally, R. Zoughi, and J. C. Bolomey, "Embedded modulated dipole scattering for near-field microwave inspection of concrete: Preliminary investigation," in *Proc. SPIE'99 Subsurface Sensors Applications Conf.*, vol. 3752, Denver, CO, Jul. 18–23, 1999, pp. 208–214.
[21] D. Hughes, "Development of the embedded modulated scattering technique for dielectric material characterization," M.S. thesis, Electrical and Computer Engineering Dept., Univ. of Missouri-Rolla, Rolla, MO, 2003.
[22] J.-C. Bolomey and F. E. Gardiol, *Engineering Applications of the Modulated Scatterer Technique*. Boston, MA: Artech House, 2001.
[23] J. H. Richmond, "A reaction theorem and its application to antenna impedance calculations," *IRE Trans. Antennas Propag.*, vol. AP-9, pp. 515–520, Nov. 1961.
[24] P. S. Carter, "Circuit relations in radiating systems and applications to antenna problems," *Proc. IRE*, vol. 20, pp. 1004–1041, Jun. 1932.
[25] C. A. Balanis, *Antenna Theory and Design*. New York: Wiley, 1982.
[26] N. Marcuvitz, *Waveguide Handbook*. New York: McGraw-Hill, 1951.
[27] D. M. Pozar, *Microwave Engineering*. New York: Wiley, 1998.
[28] C. A. Balanis, *Advanced Engineering Electromagnetics*. New York: Wiley, 1989.
[29] E. H. Newman, "An overview of the hybrid MM/Green's function method in electromagnetics," *Proc. IEEE*, vol. 76, pp. 270–282, Mar. 1988.
[30] R. F. Harrington, *Field Computation by Moment Methods*. New York: Macmillian, 1968.
[31] J. Moore and R. Pizer, *Moment Method in Electromagnetics: Techniques and Application*. New York: Wiley, 1984.
[32] H. E. King, "Mutual impedance of unequal length of antennas in echelon," *IRE Trans. Antennas Propag.*, vol. AP-5, pp. 306–313, Jul. 1957.
[33] L. D. Bamford, P. S. Hall, and A. Fray, "Calculation of antenna mutual coupling from radiated far fields," in *Proc. 2nd Int. Conf. Computation Electromagnetics*, Apr. 12–14, 1994, pp. 263–266.
[34] H. C. Baker and A. H. LaGrone, "Digital computation of the mutual impedance between thin dipoles," *IRE Trans. Antennas Propag.*, vol. AP-10, pp. 172–178, Mar. 1962.
[35] C. D. Taylor, E. A. Aronson, and C. W. Harrison Jr., "Theory of coupled monopoles," *IEEE Trans. Antennas Propag.*, vol. AP-18, pp. 360–366, May 1970.
[36] *PIN Diodes for RF Switching and Attenuating, Technical Data Sheet*, Agilent Technologies, 2000.
[37] *Applications of PIN Diodes, Application Note*, Agilent Technologies, 1999.
[38] D. Hughes and R. Zoughi, "Near-field microwave and embedded modulated scattering technique (MST) for dielectric characterization of materials," in *Proc. 29th Annu. Review Progress in Quantitative Nondestructive Evaluation*, vol. 22A, Bellingham, WA, Jul. 14–19, 2002, pp. 443–448.

Dana Hughes photograph and biography not available at the time of publication.

Reza Zoughi (S'85–M'86–SM'93) received the B.S.E.E., M.S.E.E., and Ph.D. degrees in electrical engineering (radar remote sensing, radar systems, and microwaves) from the University of Kansas, Lawrence, where from 1981 until 1987, he was with the Radar Systems and Remote Sensing Laboratory. Currently, he is the Schlumberger Distinguished Professor of Electrical and Computer Engineering at the University of Missouri-Rolla (UMR). Prior to joining UMR in January 2001 and since 1987, he was with the Electrical and Computer Engineering Department, Colorado State University (CSU), where he was a Professor and established the Applied Microwave Nondestructive Testing Laboratory (*amntl*). His current areas of research include developing new nondestructive techniques for microwave and millimeter wave inspection and testing of materials (NDT), developing new electromagnetic probes to measure characteristic properties of material at microwave frequencies, and developing embedded modulated scattering techniques for NDT purposes in particular for complex composite structures. He was Business Challenge Endowed Professor of Electrical and Computer Engineering from 1995 to 1997 while with CSU. He has published more than 300 journal publications, conference proceedings and presentations, technical reports, and overview articles. He is the author of *Microwave Nondestructive Testing and Evaluation Principles* (Norwell, MA: Kluwer Academic, 2000) and a coauthor (with A. Bahr and N. Qaddoumi) of a chapter on microwave techniques in *Nondestructive Evaluation: Theory, Techniques, and Applications* edited by P. J. Shull (New York: Marcel and Dekker, 2002). He has received seven patents in the field of microwave nondestructive testing and evaluation. He has given numerous invited talks on the subject of microwave nondestructive testing and evaluation. He is an Associate Technical Editor for *Research in Nondestructive Evaluation* and *Materials Evaluation* and the Guest Associate Editor for the Special Microwave NDE Issue of *Research in Nondestructive Evaluation*. He was Co-Guest Editor for the Special Issue of *Subsurface Sensing Technologies and Applications: Advances and Applications in Microwave and Millimeter Wave Nondestructive Evaluation*. He was the Research Symposium Coxhair for the American Society for Nondestructive Testing (ASNT) Spring Conference and 11th Annual Research Symposium in March 2002 in Portland, Oregon.

Dr. Zoughi is a member of Sigma Xi, Eta Kappa Nu and the American Society for Nondestructive Testing (ASNT). has received two Outstanding Teaching Commendations, an Outstanding Teaching Award, and the Dean of Engineering Excellence in Teaching Award from UMR. He was voted the Most Outstanding Teaching Faculty Member seven times by the junior and senior students at the Electrical and Computer Engineering Department, CSU. He received the College of Engineering Abell Faculty Teaching Award in 1995. He is the 1996 recipient of the Colorado State Board of Agriculture Excellence in Undergraduate Teaching Award. He was an Honored Researcher for seven years by the Colorado State University Research Foundation. He is an Associate Technical Editor for the IEEE RANSACTIONS ON INSTRUMENTATION AND MEASUREMENT and was Technical Chair for the IEEE Instrumentation and Measurement Technology Conference (IMTC2003) in May 2003 in Vail, CO. He was Guest Editor for the IMTC2003 special issue of the IEEE TRANSACTIONS ON INSTRUMENTATION AND MEASUREMENT. He is a member of the Administrative Committee of the IEEE Instrumentation and Measurement Society (2005–2008).